

Is charge order induced near an antiferromagnetic quantum critical point?

Xiaoyu Wang,¹ Yuxuan Wang,² Yoni Schattner,³ Erez Berg,⁴ and Rafael M. Fernandes¹

¹*School of Physics and Astronomy, University of Minnesota, Minneapolis, MN 55455*

²*School of Physics and Astronomy, University of Illinois, Urbana-Champaign, IL 61801*

³*Weizmann Institute of Science, Rehovot 7610001, Israel*

⁴*Department of Physics, University of Chicago, Chicago, IL 60637*

We investigate the interplay between charge order and superconductivity near an antiferromagnetic quantum critical point using sign-problem-free Quantum Monte Carlo simulations. We establish that, when the electronic dispersion is particle-hole symmetric, the system has an emergent SU(2) symmetry that implies a degeneracy between d -wave superconductivity and charge order with d -wave form factor. Deviations from particle-hole symmetry, however, rapidly lift this degeneracy, despite the fact that the SU(2) symmetry is preserved at low energies. As a result, we find a strong suppression of charge order caused by the competing, leading superconducting instability. Across the antiferromagnetic phase transition, we also observe a shift in the charge order wave-vector from diagonal to axial. We discuss the implications of our results to the universal phase diagram of antiferromagnetic quantum-critical metals and to the elucidation of the charge order experimentally observed in the cuprates.

The phase diagrams of a number of strongly correlated materials display putative quantum critical points (QCP), in which the transition temperature of an electronically ordered state is suppressed to zero. In systems displaying antiferromagnetic (AFM) order, such as heavy fermions, cuprates, and iron pnictides, unconventional superconductivity (SC) is found to emerge near the QCP [1]. Although it is well established that the interactions mediated by fluctuations near an AFM-QCP favor a sign-changing SC gap, the extent to which this physics describes the actual materials remains widely debated. In this context, analytical investigations of metallic AFM-QCP in two dimensions revealed a surprising result: the same electronic interaction that promotes sign-changing SC also promotes an unusual sign-changing bond charge order (CO) [2–6]. This magnetic mechanism for CO is sharply distinct from the usual mechanisms involving phonons and Fermi surface nesting. Taken at face value, this result would suggest that CO should emerge generically in the phase diagrams of AFM systems.

These theoretical results were brought to the spotlight by the experimental observation of sign-changing bond CO in cuprate high- T_c superconductors [7–19], spurring many ideas on the interplay between AFM-QCP, SC, and CO [5, 6, 20–23]. It has been proposed, for instance, that the pseudogap physics is a manifestation of a more fundamental symmetry between SC and CO near an AFM-QCP [4]. However, most of these theoretical works have relied on certain uncontrolled approximations, which are required for an analytical treatment of an AFM-QCP in a metal. The fundamental question about the universality of CO near an AFM-QCP, and the more specific question about the relevance of this result to explain charge order in cuprates, beg for unbiased methods to probe this phenomenon.

In this paper, we employ the determinantal Quantum Monte Carlo (QMC) method to address these questions.

We consider the two-band version of the spin-fermion model, for which the QMC does not suffer from the fermionic sign-problem [24]. The spin-fermion model [25] consists of free electrons coupled to an AFM order parameter tuned to its quantum critical point. Analytical and sign-problem-free QMC calculations have established the existence of a SC dome surrounding the AFM-QCP in the spin-fermion model [25, 26]. As for CO, an emergent SU(2) symmetry between CO and SC was found analytically within an approximation that considers only the vicinity of the AFM hot spots – the points on the Fermi surface which are separated by the AFM wave-vector $\mathbf{Q}_{\text{AFM}} = (\pi, \pi)$ [3, 4]. The resulting CO wave-vector lies along the diagonal of the Brillouin zone, $\mathbf{Q}_{\text{CO}} = (Q_0, Q_0)$, with $\sqrt{2}Q_0$ being the distance between hot spots in momentum space. CO with axial wave-vectors $(Q_0, 0)$ and/or $(0, Q_0)$, which are those experimentally observed in cuprates, has also been proposed [5, 27, 28] within the spin-fermion model. Although QMC investigations have not yet found CO in the spin-fermion model, they have focused on very narrow parameter regimes [26], or were performed in the superconducting phase [29].

Here, we report QMC results on the spin-fermion model showing the existence of an SU(2) symmetry between CO and SC near the AFM-QCP when the non-interacting band structure has particle-hole symmetry. This SU(2) symmetry implies a degeneracy between SC and CO, manifested by a sharp enhancement of both susceptibilities as the AFM-QCP is approached. This result demonstrates the non-trivial mechanism of magnetically-mediated CO, and establishes that the same interaction that promotes SC in the spin-fermion model is also capable of promoting CO.

As the particle-hole symmetry of the non-interacting band dispersion is broken, however, we find that while the enhancement of the SC susceptibility is preserved,

the CO susceptibility shows a very weak enhancement near the QCP. Furthermore, near the onset of SC, the CO susceptibility is even suppressed with respect to its non-interacting value, signaling a strong competition between these two states already in the fluctuating regime. This happens even though the SU(2) symmetry is preserved locally at the hot spots. The fragility of the CO-SC degeneracy implies that CO near an AFM-QCP is not a universal phenomenon, but instead requires a fine-tuned band structure that goes beyond just hot-spot properties. We also investigate the wave-vector for which the CO susceptibility is maximal. When CO and SC are degenerate, the wave-vector is diagonal, in agreement with the analytical approximations. However, once CO and SC are no longer degenerate, the wave-vector tends to change from diagonal to axial as the AFM-QCP is approached. This is consistent with theoretical proposals that axial CO is favored over the diagonal one if the anti-nodal region of the Brillouin zone is gapped [30, 31]. Finally, we discuss the implications of our results to materials that display putative AFM-QCPs and their relevance to understand CO in the cuprates.

The spin-fermion model is a low-energy model describing electrons interacting via the exchange of AFM fluctuations. In its two-band version (whose physics has been argued to be similar to the one-band version [32]), the model is described by the following action, $S = S_\psi + S_\phi + S_\lambda$, defined on a two-dimensional square lattice:

$$\begin{aligned} S_\psi &= \int_{\tau, \mathbf{r}, \mathbf{r}'} \sum_{i=c,d} [(\partial_\tau - \mu) \delta_{\mathbf{r}\mathbf{r}'} - t_{i, \mathbf{r}\mathbf{r}'}] \psi_{i, \mathbf{r}\alpha}^\dagger \psi_{i, \mathbf{r}'\alpha} \\ S_\phi &= \frac{1}{2} \int_{\tau, \mathbf{r}} \left[\frac{1}{v_s^2} (\partial_\tau \phi)^2 + (\nabla \phi)^2 + r_0 \phi^2 + \frac{u}{2} (\phi^2)^2 \right] \\ S_\lambda &= \lambda \int_{\tau, \mathbf{r}} e^{i\mathbf{Q}_{\text{AFM}} \cdot \mathbf{r}} \phi \cdot (\psi_{c, \mathbf{r}\alpha}^\dagger \boldsymbol{\sigma}_{\alpha\beta} \psi_{d, \mathbf{r}\beta} + h.c.) \end{aligned} \quad (1)$$

Here, $\int_{\tau, \mathbf{r}}$ is shorthand for $\int d\tau \sum_{\mathbf{r}}$, $\tau \in [0, \beta)$ is the imaginary time, and $\beta = 1/T$ is the inverse temperature. The action S_ψ describes the fermionic degrees of freedom, with the operator $\psi_{i, \mathbf{r}\alpha}$ annihilating an electron of spin α at site \mathbf{r} and band i . Summation over α, β is implied. There are two different bands, labeled c and d . The band dispersion is parametrized by the chemical potential μ and the hopping amplitudes $t_{i, \mathbf{r}\mathbf{r}'}$. Here, we consider only nearest-neighbor hopping and set $t_{c,x} = t_{d,y} \equiv t_x$ and $t_{c,y} = t_{d,x} \equiv t_y$ to enforce the system to remain invariant under a 90° rotation followed by a $c \leftrightarrow d$ exchange. The action S_ϕ describes the spin degrees of freedom, with the bosonic field ϕ denoting the antiferromagnetic order parameter with ordering wave-vector $\mathbf{Q}_{\text{AFM}} = (\pi, \pi)$, and $\boldsymbol{\sigma}$ denoting Pauli matrices. The parameter r_0 tunes the AFM transition to $T = 0$ at $r_0 = r_c$, whereas v_s and u describe the stiffness of AFM temporal and amplitude fluctuations, respectively. To save computational time,

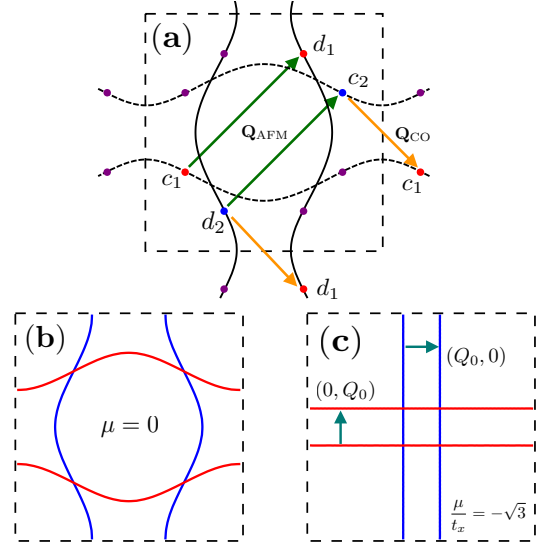


Figure 1. (a) Schematic Fermi surface of the spin-fermion model with two bands (c , dashed line, and d , solid line). Hot spots are marked by solid symbols. Two pairs of hot spots (c_1, d_1) and (c_2, d_2) are highlighted to illustrate the relationship between the AFM wave-vector \mathbf{Q}_{AFM} and the CO wave-vector \mathbf{Q}_{CO} . The band dispersions used in our QMC calculations are shown in (b) (particle-hole symmetric dispersion, $\mu = 0$, with $t_y = t_x/2$) and (c) (particle-hole asymmetric dispersion, $\mu/t_x = -\sqrt{3}$, with $t_y = 0$). Changing μ tunes the CO wave-vector $\mathbf{Q}_{\text{CO}} = (Q_0, Q_0)$ since $Q_0 = 2 \arccos \frac{\mu}{t_x}$.

we follow previous works and consider easy-plane anti-ferromagnetism, i.e. $\phi = (\phi_x, \phi_y)$ [26, 32, 33]. The action S_λ couples spins and fermions via the parameter λ . The two-band structure of the model ensures the absence of the sign problem in our simulations [24].

The fermionic, magnetic, and superconducting properties of this model have been thoroughly studied recently, revealing a SC dome surrounding the QCP [26, 33]. In particular, the SC order parameter Δ was found to have a “ d -wave” symmetry, i.e. to change its sign between the two bands: $\Delta = \int_{\tau, \mathbf{r}} i \sigma_{\alpha\beta}^y (\psi_{c, \mathbf{r}\alpha} \psi_{c, \mathbf{r}\beta} - \psi_{d, \mathbf{r}\alpha} \psi_{d, \mathbf{r}\beta})$. The CO order parameter ρ investigated here also has opposite signs in the two-bands (and is thus analogous to the d -wave bond CO in the one-band version of the model):

$$\rho = \int_{\tau, \mathbf{r}} e^{i\mathbf{Q}_{\text{CO}} \cdot \mathbf{r}} \sigma_{\alpha\beta}^0 (\psi_{c, \mathbf{r}\alpha}^\dagger \psi_{c, \mathbf{r}\alpha} - \psi_{d, \mathbf{r}\alpha}^\dagger \psi_{d, \mathbf{r}\alpha}). \quad (2)$$

where \mathbf{Q}_{CO} is the CO wave-vector. Analytical studies of the spin-fermion model found a special symmetry relating the SC and CO order parameters under an approximation that focuses on the hot spots of the model, i.e. the Fermi surface points separated by $\mathbf{Q}_{\text{AFM}} = (\pi, \pi)$ [3–5]. In the two-band version of the model, each hot spot of a given pair (c_i, d_i) is located on a different band, as shown in Fig. 1. According to [3, 4, 34], the hot-spots model with linearized dispersions has an emergent symmetry that rotates the SC order param-

ter, $\Delta = i\sigma_{\alpha\beta}^y (\psi_{c1,\alpha}\psi_{c2,\beta} - \psi_{d1,\alpha}\psi_{d2,\beta})$, onto the CO order parameter, $\rho = \sigma_{\alpha\beta}^0 (\psi_{c1,\alpha}^\dagger\psi_{c2,\beta} - \psi_{d1,\alpha}^\dagger\psi_{d2,\beta})$. Note that this CO has a diagonal wave-vector $\mathbf{Q}_{\text{CO}} \equiv (Q_0, Q_0)$ which separates two hot spots belonging to different pairs but to the same band (see Fig. 1). Our goal here is to investigate: (i) to what extent does this symmetry play a role in the vicinity of an AFM-QCP, and (ii) more broadly, is CO a generic feature near such a QCP. To this end, we perform a systematic investigation of the SC and CO susceptibilities in the two-band spin-fermion model.

We choose as our starting point the parameters for which the symmetry of the low-energy hot-spots model discussed above is promoted to an exact lattice symmetry. This corresponds to the case where the c and d bands are particle-hole symmetric, i.e. $\mu = 0$. This allows us to systematically study the effect of breaking the particle-hole symmetry at the lattice level. For $\mu = 0$, the electronic action for a given AFM field configuration – corresponding to the S_ψ and S_λ terms of the action in Eq. (1) [3] – is invariant under a rotation in particle-hole space, $\psi_{i,\mathbf{r}\alpha} \rightarrow e^{i\mathbf{Q}_{\text{AFM}} \cdot \mathbf{r}} (i\sigma_{\alpha\beta}^y) \psi_{i,\mathbf{r}\beta}^\dagger$. This invariance can be seen by constructing a four-dimensional spinor that combines rotated and non-rotated operators at each band, $\Psi_{i,\mathbf{r}} \equiv (\psi_{i,\mathbf{r}\uparrow}, \psi_{i,\mathbf{r}\downarrow}, e^{i\mathbf{Q}_{\text{AFM}} \cdot \mathbf{r}} \psi_{i,\mathbf{r}\uparrow}^\dagger, -e^{i\mathbf{Q}_{\text{AFM}} \cdot \mathbf{r}} \psi_{i,\mathbf{r}\downarrow}^\dagger)^T$. In this representation, when $\mu = 0$, the Hamiltonian commutes with all all SU(2) generators τ in particle-hole space. Importantly, the SC and CO order parameters form a three-component vector $\Phi \equiv (\Re\Delta, \Im\Delta, \rho)$ in this space, which couples to the electrons as $\sum_{\mathbf{r}} e^{i\mathbf{Q}_{\text{AFM}} \cdot \mathbf{r}} \Phi \cdot (\sigma_0 \otimes \tau) (\Psi_{c,\mathbf{r}}^\dagger \Psi_{c,\mathbf{r}} - \Psi_{d,\mathbf{r}}^\dagger \Psi_{d,\mathbf{r}})$. Note that $\mathbf{Q}_{\text{CO}} = \mathbf{Q}_{\text{AFM}} = (\pi, \pi)$, enforcing ρ to be real. As a result, an enhancement of the SC susceptibility also implies an equally strong enhancement in the CO channel, since the two order parameters are related by rotations in the SU(2) particle-hole space, and the Hamiltonian is invariant under these rotations. This symmetry is analogous to the degeneracy between SC and CO observed in the half-filled negative- U Hubbard model [35]. Here, however, both the SC and CO have a d -wave symmetry.

To demonstrate the existence of this SU(2) symmetry for $\mu = 0$, we perform QMC simulations on a square lattice of size $L = 12$. Additional details of the QMC procedure can be found elsewhere [26]. All energies are expressed in terms of the hopping $t_x \equiv t$ and the parameters are set to $v_s = 2t$, $u = t^{-1}$, $\lambda^2 = 4t$, and $t_y = t/2$, resulting in the Fermi surface illustrated in Fig. 1(b) (the results are the same for other values of t_y , see Supplementary Material). Fig. 2(a) shows the SC susceptibility χ_{SC} , the CO susceptibility $\chi_{\text{CO}}^{\text{diag}}$ with diagonal wave-vector $\mathbf{Q}_{\text{CO}} = (Q_0, Q_0)$, where $Q_0 = \pi$, and the CO susceptibility $\chi_{\text{CO}}^{\text{axial}}$ with axial wave-vector $\mathbf{Q}_{\text{CO}} = (Q_0, 0)/(0, Q_0)$ as a function of the distance to the AFM-QCP for $\beta t = 12$. The position r_c of the

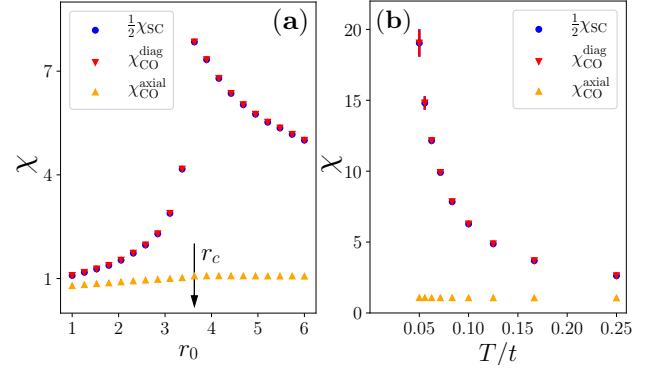


Figure 2. SC susceptibility χ_{SC} (circles) and CO susceptibilities for diagonal wave-vector $\mathbf{Q}_{\text{CO}} = (Q_0, Q_0)$, $\chi_{\text{CO}}^{\text{diag}}$ (triangles), and axial wave-vector $\mathbf{Q}_{\text{CO}} = (Q_0, 0)/(0, Q_0)$, $\chi_{\text{CO}}^{\text{axial}}$ (inverted triangles), as function of: (a) the distance $r_0 - r_c$ to the AFM-QCP (fixed temperature $\beta t = 12$); and (b) temperature T/t (fixed $r_0 = r_c$ at the AFM-QCP). The particle-hole symmetric dispersion used here is that of Fig. 1(b).

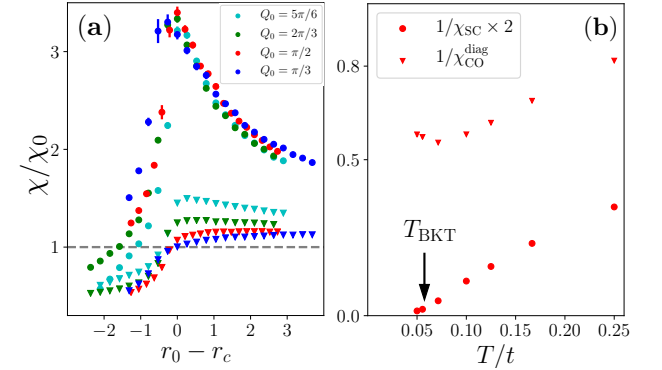


Figure 3. (a) SC (circles) and diagonal CO (triangles) susceptibilities, normalized by their non-interacting values, as a function of the distance to the QCP $r_0 - r_c$ and for a fixed temperature $\beta t = 10$. The dispersion is represented in Fig. 1(c), with different values of the wave-vector Q_0 (shown in the inset). Panel (b) shows the temperature dependence of the inverse susceptibilities at the AFM-QCP ($r_0 = r_c$) for $\mu/t = -\sqrt{2}$ ($Q_0 = \pi/2$).

AFM-QCP was determined via the AFM susceptibility [32]. The degeneracy between diagonal CO and SC is evident, as well as the enhancement of both susceptibilities at the AFM-QCP. The fact that $\chi_{\text{SC}} = 2\chi_{\text{CO}}^{\text{diag}}$ is because the complex SC order parameter has two components whereas the real CO order parameter has one. In contrast, the axial CO susceptibility remains small and nearly unaffected by the proximity to the QCP. Fig. 2(b), which shows the behavior at the QCP, confirms that the degeneracy is present at all temperatures.

We now proceed to investigate whether there is a remnant near-degeneracy between SC and CO when particle-hole symmetry is broken ($\mu \neq 0$). In this case, although there is no lattice SU(2) symmetry, an approx-

imate SU(2) symmetry of the low energy theory near the hot spots is preserved [34][36]. To favor the CO state, we consider one-dimensional dispersions ($t_y = 0$), as shown in Fig. 1(c), although the results are similar for finite t_y (see Supplementary Material). To be able to assess the relevant CO wave-vectors $\mathbf{Q}_{\text{CO}} = (Q_0, Q_0)$ in the finite-size QMC simulations, we choose μ values that yield commensurate $Q_0 \equiv 2 \arccos \frac{-\mu}{2t} = \frac{2\pi n}{L}$, namely: $\mu/t = -2 \cos \frac{5\pi}{12} \approx -0.52$ ($Q_0 = 5\pi/6$), $\mu/t = -1$ ($Q_0 = 2\pi/3$), $\mu/t = -\sqrt{2}$ ($Q_0 = \pi/2$), and $\mu/t = -\sqrt{3}$ ($Q_0 = \pi/3$).

Figure 3(a) displays the behavior of χ_{SC} and $\chi_{\text{CO}}^{\text{diag}}$, normalized by their non-interacting ($\lambda = 0$) value, as a function of the distance to the QCP for different values of μ . While the sharp enhancement of χ_{SC} at $r_0 = r_c$ is preserved, the enhancement of $\chi_{\text{CO}}^{\text{diag}}$ is small for $r_0 > r_c$. This enhancement of $\chi_{\text{CO}}^{\text{diag}}$ is larger the closer μ is to zero, i.e. the closer the global lattice SU(2) symmetry is to be restored. The CO-SC degeneracy observed for $\mu = 0$ is thus removed, with SC clearly winning over CO. The competition between the two orders is highlighted in Fig. 3(b), where the T dependences of $1/\chi_{\text{SC}}$ and $1/\chi_{\text{CO}}^{\text{diag}}$ are plotted at the QCP, $r_0 = r_c$. Interestingly, right above the Berezinskii-Kosterlitz-Thouless superconducting transition temperature (extracted from the superfluid density, see Ref. [32]), $\chi_{\text{CO}}^{\text{diag}}$ reverses its trend and starts to decrease upon lowering the temperature. This provides evidence that the competition between SC and CO takes place already in the fluctuating regime.

Another important result from our QMC simulations is that, when the AFM hot spots are near the antinodal region of the Brillouin zone (i.e., $(\pi, 0)/(0, \pi)$), the CO wave-vector tends to shift from diagonal to axial inside the AFM phase. To illustrate this, in Fig. 4 we plot $\chi_{\text{CO}}(\mathbf{q})$ for the system with $\mu/t = -\sqrt{2}$ ($Q_0 = \pi/2$) in the disordered phase ($r_0 > r_c$), at the QCP ($r_0 = r_c$), and in the AFM phase ($r_0 < r_c$). Results for other fillings are discussed in the Supplementary Material. The tendency of shifting \mathbf{Q}_{CO} from diagonal (above the QCP) to axial (below the QCP) is evident. To quantify this behavior, we plot in Fig. 4(d) the ratio between the maxima of χ_{CO} along the diagonal and axial directions as function of r_0 for different temperatures. Upon approaching the QCP from the disordered side, and upon decreasing the temperature, this ratio increases due to the enhancement of diagonal CO by quantum critical AFM fluctuations. Below the QCP and inside the AFM phase ($r_0 < r_c$), however, the maximum of $\chi_{\text{CO}}(\mathbf{q})$ quickly shifts to the axial direction, and the temperature dependence of the ratio is the opposite as in the disordered side. This effect is consistent with theoretical proposals that axial CO is favored over diagonal CO if the antinodal regions of the Brillouin zone are gapped (e.g. by AFM order here or by a more exotic pseudogap state [30, 31]).

In summary, we showed that the spin-fermion model

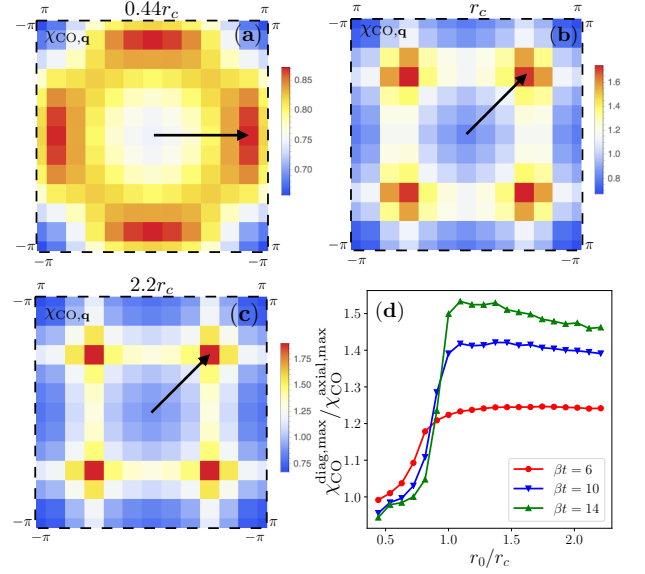


Figure 4. Panels (a)-(c) show the momentum dependence of the CO susceptibility $\chi_{\text{CO}}(\mathbf{q})$ in the AFM phase (a), at the QCP (b), and in the disordered phase (c) for $\beta t = 14$. The dispersion is represented in Fig. 1(c) with $\mu/t = -\sqrt{2}$. (b) Ratio of the maximum values of $\chi_{\text{CO}}(\mathbf{q})$ along the diagonal direction, $\mathbf{q} = (q, q)$, and along the axial direction, $\mathbf{q} = (q, 0)$, for different inverse temperatures β (inset), as function of the distance to the QCP at $r_0 = r_c$.

with particle-hole symmetric bands has a global SU(2) symmetry that relates d -wave SC and d -wave CO. The breaking of this particle-hole symmetry strongly suppresses the CO susceptibility, even though the SU(2) symmetry is still present near the hot spots. Compared with previous QMC investigations of the spin-fermion model, which showed that the SC instability is governed by the hot spots [32], our results indicate that the CO instability is instead governed by the full electronic dispersion. Such an asymmetry between CO and SC implies that CO is not a universal phenomenon associated with AFM quantum criticality, in contrast to SC.

The applicability of these results to specific materials – and particularly the cuprates – remains an open question. On the one hand, the CO observed in most cuprates only acquires a substantially long correlation length once SC is fully suppressed, and CO fluctuations are found to be suppressed by the onset of SC [8, 18, 19]. Furthermore, in the pseudogap state where CO is experimentally observed, the CO wave-vector is axial, and not diagonal. All these observations seem at least qualitatively consistent with our results for systems without particle-hole symmetric band dispersions. On the other hand, in hole-doped cuprates, AFM fluctuations become weaker as the system approaches optimal doping and CO is observed. The fact that CO is strongest near a specific doping close to $1/8$, where AFM fluctuations are not particularly enhanced, suggests that lattice commensuration

effects, rather than AFM criticality, may play an important role in these systems.

We thank A. Chubukov for fruitful discussions. X.W. and R.M.F. were supported by the U.S. Department of Energy, Office of Science, Basic Energy Sciences, under Award number de-sc0012336. R.M.F. also acknowledges partial support from the Research Corporation for Science Advancement via the Cottrell Scholar Award, and X.W. acknowledges support from the Doctoral Dissertation Fellowship offered by the University of Minnesota. Y.W. is supported by the Gordon and Betty Moore Foundation's EPiQS Initiative through Grant No. GBMF4305 at the University of Illinois. R.M.F. and X.W. thank the Minnesota Supercomputing Institute (MSI) at the University of Minnesota, where part of the numerical computations was performed.

-
- [1] D. J. Scalapino, *Rev. Mod. Phys.* **84**, 1383 (2012).
 - [2] M. A. Metlitski and S. Sachdev, *New Journal of Physics* **12**, 105007 (2010).
 - [3] M. A. Metlitski and S. Sachdev, *Phys. Rev. B* **82**, 075128 (2010).
 - [4] K. B. Efetov, H. Meier, and C. Pepin, *Nat Phys* **9**, 442 (2013).
 - [5] Y. Wang and A. Chubukov, *Phys. Rev. B* **90**, 035149 (2014).
 - [6] A. Allais, J. Bauer, and S. Sachdev, *Phys. Rev. B* **90**, 155114 (2014).
 - [7] T. Wu, H. Mayaffre, S. Kramer, M. Horvatic, C. Berthier, W. N. Hardy, R. Liang, D. A. Bonn, and M.-H. Julien, *Nature* **477**, 191 (2011).
 - [8] J. Chang, E. Blackburn, A. T. Holmes, N. B. Christensen, J. Larsen, J. Mesot, R. Liang, D. A. Bonn, W. N. Hardy, A. Watenphul, M. v. Zimmermann, E. M. Forgan, and S. M. Hayden, *Nat Phys* **8**, 871 (2012).
 - [9] A. J. Achkar, R. Sutarto, X. Mao, F. He, A. Frano, S. Blanco-Canosa, M. Le Tacon, G. Ghiringhelli, L. Braicovich, M. Minola, M. Moretti Sala, C. Mazzoli, R. Liang, D. A. Bonn, W. N. Hardy, B. Keimer, G. A. Sawatzky, and D. G. Hawthorn, *Phys. Rev. Lett.* **109**, 167001 (2012).
 - [10] G. Ghiringhelli, M. Le Tacon, M. Minola, S. Blanco-Canosa, C. Mazzoli, N. B. Brookes, G. M. De Luca, A. Frano, D. G. Hawthorn, F. He, T. Loew, M. M. Sala, D. C. Peets, M. Salluzzo, E. Schierle, R. Sutarto, G. A. Sawatzky, E. Weschke, B. Keimer, and L. Braicovich, *Science* **337**, 821 (2012).
 - [11] E. Blackburn, J. Chang, M. Hücker, A. T. Holmes, N. B. Christensen, R. Liang, D. A. Bonn, W. N. Hardy, U. Rütt, O. Gutowski, M. v. Zimmermann, E. M. Forgan, and S. M. Hayden, *Phys. Rev. Lett.* **110**, 137004 (2013).
 - [12] N. Doiron-Leyraud, S. Lepault, O. Cyr-Choinière, B. Vignolle, G. Grissonnanche, F. Laliberté, J. Chang, N. Barišić, M. K. Chan, L. Ji, X. Zhao, Y. Li, M. Greven, C. Proust, and L. Taillefer, *Phys. Rev. X* **3**, 021019 (2013).
 - [13] D. LeBoeuf, S. Kramer, W. N. Hardy, R. Liang, D. A. Bonn, and C. Proust, *Nat Phys* **9**, 79 (2013).
 - [14] R. Comin, A. Frano, M. M. Yee, Y. Yoshida, H. Eisaki, E. Schierle, E. Weschke, R. Sutarto, F. He, A. Soumyanarayanan, Y. He, M. Le Tacon, I. S. Elfimov, J. E. Hoffman, G. A. Sawatzky, B. Keimer, and A. Damascelli, *Science* **343**, 390 (2014).
 - [15] K. Fujita, C. K. Kim, I. Lee, J. Lee, M. H. Hamidian, I. A. Firmo, S. Mukhopadhyay, H. Eisaki, S. Uchida, M. J. Lawler, E.-A. Kim, and J. C. Davis, *Science* **344**, 612 (2014).
 - [16] E. H. da Silva Neto, P. Aynajian, A. Frano, R. Comin, E. Schierle, E. Weschke, A. Gyenis, J. Wen, J. Schneeloch, Z. Xu, S. Ono, G. Gu, M. Le Tacon, and A. Yazdani, *Science* **343**, 393 (2014).
 - [17] A. Mesaros, K. Fujita, S. D. Edkins, M. H. Hamidian, H. Eisaki, S.-i. Uchida, J. C. S. Davis, M. J. Lawler, and E.-A. Kim, *Proceedings of the National Academy of Sciences* **113**, 12661 (2016).
 - [18] H. Jang, W.-S. Lee, H. Nojiri, S. Matsuzawa, H. Yasumura, L. Nie, A. V. Maharaj, S. Gerber, Y.-J. Liu, A. Mehta, D. A. Bonn, R. Liang, W. N. Hardy, C. A. Burns, Z. Islam, S. Song, J. Hastings, T. P. Devereaux, Z.-X. Shen, S. A. Kivelson, C.-C. Kao, D. Zhu, and J.-S. Lee, *Proceedings of the National Academy of Sciences* **113**, 14645 (2016).
 - [19] J. Chang, E. Blackburn, O. Ivashko, A. T. Holmes, N. B. Christensen, M. Hücker, R. Liang, D. A. Bonn, W. N. Hardy, U. Rütt, M. v. Zimmermann, E. M. Forgan, and S. M. Hayden, *Nature Communications* **7**, 11494 (2016).
 - [20] S. Bulut, W. A. Atkinson, and A. P. Kampf, *Phys. Rev. B* **88**, 155132 (2013).
 - [21] S. Sachdev and R. La Placa, *Phys. Rev. Lett.* **111**, 027202 (2013).
 - [22] L. E. Hayward, D. G. Hawthorn, R. G. Melko, and S. Sachdev, *Science* **343**, 1336 (2014).
 - [23] S. Caprara, C. Di Castro, G. Seibold, and M. Grilli, *Phys. Rev. B* **95**, 224511 (2017).
 - [24] E. Berg, M. A. Metlitski, and S. Sachdev, *Science* **338**, 1606 (2012).
 - [25] A. Abanov, A. V. Chubukov, and J. Schmalian, *Advances in Physics* **52**, 119 (2003).
 - [26] Y. Schattner, M. H. Gerlach, S. Trebst, and E. Berg, *Phys. Rev. Lett.* **117**, 097002 (2016).
 - [27] H. Meier, C. Pépin, M. Einenkel, and K. B. Efetov, *Phys. Rev. B* **89**, 195115 (2014).
 - [28] D. Chowdhury and S. Sachdev, *Phys. Rev. B* **90**, 134516 (2014).
 - [29] Z.-X. Li, F. Wang, H. Yao, and D.-H. Lee, *Phys. Rev. B* **95**, 214505 (2017).
 - [30] D. Chowdhury and S. Sachdev, *Phys. Rev. B* **90**, 245136 (2014).
 - [31] W. A. Atkinson, A. P. Kampf, and S. Bulut, *New Journal of Physics* **17**, 013025 (2015).
 - [32] X. Wang, Y. Schattner, E. Berg, and R. M. Fernandes, *Phys. Rev. B* **95**, 174520 (2017).
 - [33] M. H. Gerlach, Y. Schattner, E. Berg, and S. Trebst, *Phys. Rev. B* **95**, 035124 (2017).
 - [34] Y. Wang, D. F. Agterberg, and A. Chubukov, *Phys. Rev. B* **91**, 115103 (2015).
 - [35] A. Moreo and D. J. Scalapino, *Phys. Rev. Lett.* **66**, 946 (1991).
 - [36] Technically the hot-spots symmetry is $SU(2) \times SU(2) \sim SO(4)$ and not $SU(2)$, because for $\mu \neq 0$ the CO order parameter is complex, giving rise to a

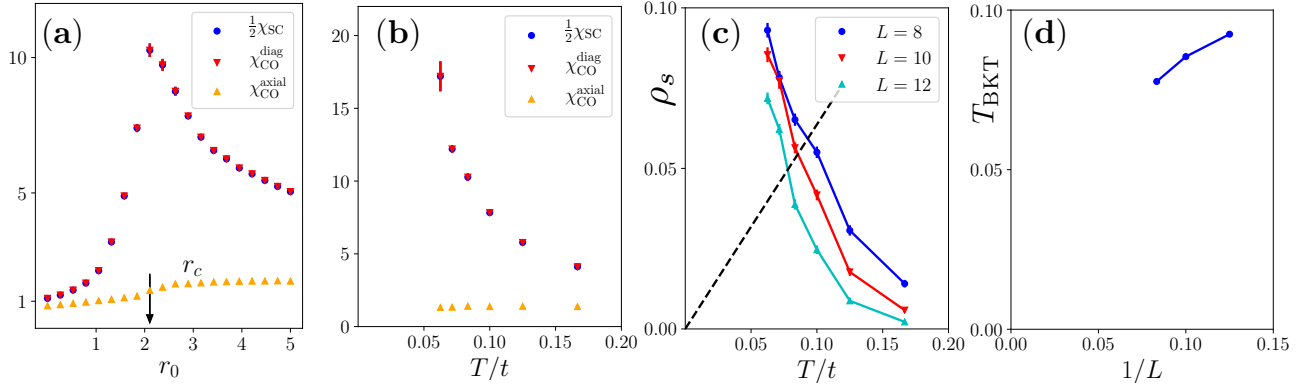


Figure S1. QMC results for the one-dimensional electronic band dispersion ($t_y = 0$) at half-filling $\mu = 0$. (a) Sign-changing SC and CO susceptibilities as a function of the distance to AFM-QCP. Results obtained for $\beta t = 12$ (b) Temperature evolution of SC and CO susceptibilities at the AFM-QCP. Both (a) and (b) are obtained for the system size $L = 12$. (c) Temperature evolution of the superfluid density at the AFM-QCP, extracted from the current-current correlation function, see Ref. [26, 32]. Different system sizes are plotted. The shift of the AFM-QCP with system size is negligible. (d) Berezinskii-Kosterlitz-Thouless transition temperature as a function of inverse system size, extracted from the superfluid density.

four-component super-vector.

Supplementary Material: “Is charge order induced near an antiferromagnetic quantum critical point?”

I. DEGENERACY BETWEEN SC AND CO AT HALF-FILLING

When the two-band spin-fermion model has the exact lattice symmetry (half-filling), the d -wave superconductivity (SC) and d -wave charge order (CO) with wave-vector $\mathbf{Q}_{\text{CO}} = (\pi, \pi)$ form a three-component super-vector. At any temperature and distance to the antiferromagnetic quantum critical point (AFM-QCP), the CO and SC susceptibilities differ by a factor of 2, corresponding to having a real CO and a complex SC order parameter. While in the main text we focused on the particular band dispersion with $t_y = t_x/2$, the CO-SC degeneracy holds for any band dispersion at half-filling ($\mu = 0$). To verify this, we also considered the purely one-dimensional band dispersion at half-filling, with $t_y = 0$. In Figure S1, we present the SC and CO susceptibilities as a function of the distance to the AFM-QCP for the inverse temperature $\beta t = 12$, as well as at various temperatures above the QCP. The SC susceptibility is rescaled by $\frac{1}{2}$. The degeneracy between SC and CO is evident.

The enlarged SU(2) symmetry also means that there is no finite-temperature Berezinskii-Kosterlitz-Thouless phase transition. In Fig. S1, we show the superfluid density as well as the extracted BKT transition temperature for system sizes $L = 8$, $L = 10$, and $L = 12$. As L increases, the superfluid density at a given temperature decreases, and that the BKT temperature shows finite size scaling. Due to computational costs, we did not go to larger system sizes. Nonetheless, the fact that T_{BKT} goes down with system size is consistent with having an enlarged symmetry. For comparison, in systems without the enlarged symmetry, T_{BKT} remains nearly saturated for these system sizes (see Ref. [32]).

II. EVOLUTION OF THE CO WAVE-VECTOR AWAY FROM HALF-FILLING

A. 1D dispersions

For a given band dispersion, we have determined the wave-vector \mathbf{Q}_{max} for which the CO susceptibility is maximal. In Fig. S2, we present the coordinates of $\mathbf{Q}_{\text{max}} = (Q_x, Q_y)$ as a function of r_0 for purely one-dimensional band dispersions ($t_y = 0$) corresponding to $Q_0 = 5\pi/6$, $Q_0 = 2\pi/3$, $Q_0 = \pi/2$, and $Q_0 = \pi/3$. The results are obtained for the inverse temperature $\beta t = 14$, and the qualitative features of the results are similar when temperature is changed.

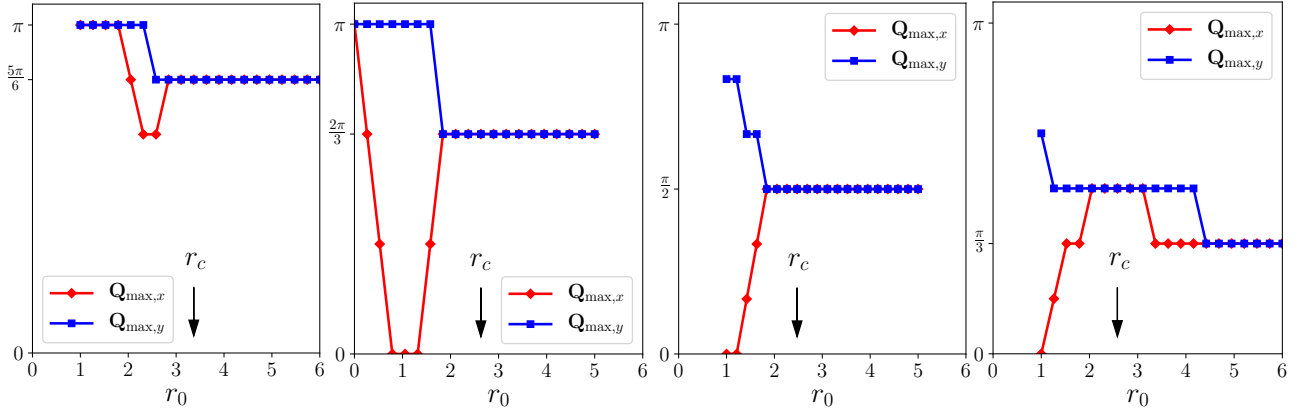


Figure S2. Maximal CO wave-vector $\mathbf{Q}_{\max} = (Q_x, Q_y)$ for one-dimensional band dispersions ($t_y = 0$). From left to right: $Q_0 = 5\pi/6$, $Q_0 = 2\pi/3$, $Q_0 = \pi/2$, and $Q_0 = \pi/3$. The inverse temperature is set to $\beta t = 14$.

With the exception of $Q_0 = \pi/3$, where the Fermi energy is small compared to the bandwidth, the shift of the maximal CO wave-vector to axial occurs inside the AFM phase, indicating that Fermi surface reconstruction plays a major role. The maximal wave-vector deep inside the AFM phase appears to be non-universal and dependent on the chemical potential. For systems close to half-filling (i.e. Q_0 close to π), the maximal wave-vector stays along the diagonal direction. However, for systems farther away from half filling, the maximal wave-vector shifts towards the axial direction.

We attribute the qualitative differences among the maximal wave-vectors of different chemical potentials to the location of the AFM hot spots. For $Q_0 = 5\pi/6$ and $Q_0 = 2\pi/3$, the hot spots are located near the diagonal directions. For $Q_0 = \pi/2$ and $Q_0 = \pi/3$, however, the hot spots are closer to the antinodal region of the Fermi surface. As a result, the AFM order can have a stronger effect on the electronic states along the diagonal or axial directions depending on the chemical potential. The diagonal-axial asymmetry of the reconstructed Fermi surface is thus responsible for the position of the maximal CO wave-vector.

B. Quasi-1D dispersions

To show that the choice of one-dimensional band dispersions is not responsible for the observed lifting of the SC-CO degeneracy and for the observed shift of the CO wave-vector from diagonal to axial, here we present results for a slightly curved band dispersion. In particular, we consider the parameters $t_y = 0.1t_x$ and $\mu = -\sqrt{3} + 2t_y$. This choice generates a small curvature to the Fermi surface while retaining the momentum points $(\frac{\pi}{6}, 0) / (0, \frac{\pi}{6})$ on the Fermi surface. In Fig. S3, we present the band dispersion for the non-interacting problem, the evolution of the CO wave-vector as the AFM-QCP is crossed, as well as the dependence of the sign-changing SC and diagonal CO susceptibilities as the AFM-QCP is approached. The results are consistent with those presented in the main text for 1D band dispersions.

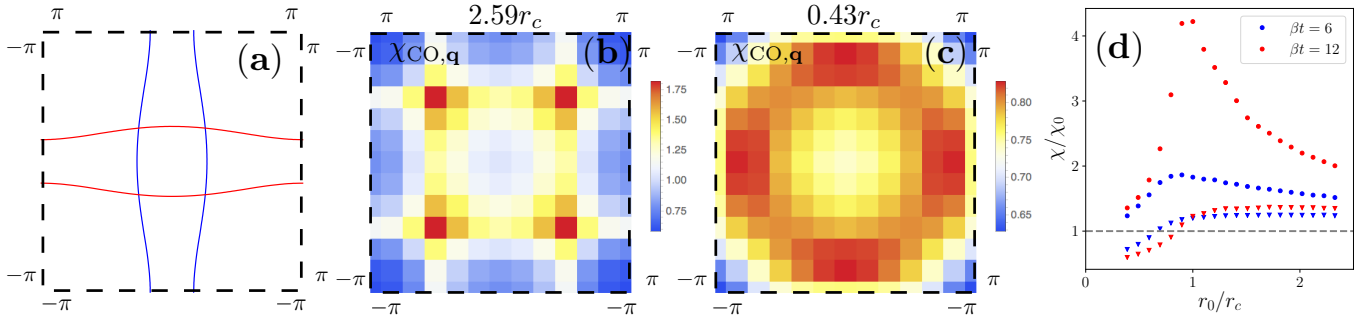


Figure S3. QMC results for the diagonal CO and SC susceptibilities for the quasi-1D band dispersion plotted in (a). Panels (b) and (c) show the CO susceptibility above and below the magnetic QCP, respectively. Panel (d) shows the r_0 dependence of the SC (diamond) and diagonal-CO (triangle) susceptibilities for temperatures $\beta t = 6$ (blue) and $\beta t = 12$ (red), demonstrating the breaking of the SC-CO degeneracy observed at half filling.